Water Air Soil Pollut (2021) 232: 213
https://doi.org/10.1007/s11270-021-05159-3

Evolution of a Deep Fluid in a Surficial Environment Using Stable Carbon and Sulfur Isotopes: Case of the Transitional Zone of the Edwards Aquifer in South Central Texas

Pride T. Abongwa · Walter Den

Received: 22 February 2021 / Accepted: 29 April 2021 / Published online: 10 May 2021

Abstract The Edwards Aquifer in south central Texas (USA) features a distinct fault line defining the freshwater and saline water zones. We aim to elucidate the evolutionary behavior of carbon and sulfur emanating from deep environments and flowing in surficial environment so as to better understand the cycling of these metals in water environments. To characterize the evolution of carbon and sulfur species in surficial environment as the fluid emanates from a deep saline aquifer, we monitored the chemical and isotopic ($\delta^{13}C_{DIC}$ and $\delta^{34}S_{SO4}$) parameters over a 700-m stretch on a stream-pond system situated on the saline-freshwater line of the Edwards Aquifer's artesian zone. A three-tier evolution process associated with the interaction of a deep saline fluid with a fresh-ponded water was observed, namely: A deep fluid control zone characterized by decreasing pH values and relatively high total dissolved solids (TDS) concentrations along the stream path; a mixing zone of the deep fluid and fresh-ponded water where the TDS concentrations showed a sharp decline and a continual decrease in pH values; and a fresh-ponded water-controlled zone with a stable pH value and low TDS concentrations. The decreasing pH values were a result of CO_2 outgassing due to the relatively high CO_2 partial pressures ($10^{-2.53}$ atm) relative to atmospheric ($10^{-3.50}$ atm) in the aqueous system, and the high TDS concentrations were attributed to the deep saline fluid emanating at the well-head. The enrichment in the $\delta^{13}C_{DIC}$ and $\delta^{34}S_{SO4}$ for the initial stream path reflects the kinetic isotopic fractionations associated with CO_2 outgassing and with the microbial conversion. The zonation of the evolutionary process indicates that (i) solutes play a critical role in the evolution of carbon and sulfur in surficial environment, (ii) kinetic and chemical fractionation are the dominant processes controlling carbon evolution, and (iii) microbial metabolism primarily controls sulfate fractionation and evolution through the conversion of sulfate to thiosulfate.

Keywords Deep saline fluids · Surficial environments · Carbon · Sulfur · Oxygen and hydrogen isotopes · CO_2 outgassing · Microbial metabolism

Highlights
- We assessed carbon and sulfur evolution from deep fluids in surficial environments.
- TDS increases over distance until interaction with fresh surface water, while pH decreases throughout.
- Carbon evolved by CO_2 outgassing, whereas sulfur evolved by microbial metabolism.
- Kinetic fractionation was associated with carbon evolution and conversion of sulfate to thiosulfate causes sulfur fractionation.
- Three tier-evolution was established: Zone 1, deep fluid control; Zone 2, mixing area; and Zone 3, freshwater dominance.

P. T. Abongwa (✉) · W. Den
Department of Mathematical, Physical, and Engineering Sciences, Texas A&M University-San Antonio, One University Way, San Antonio, TX 78224, USA
e-mail: pabongwa@tamusa.edu

1 Introduction

The Edwards Balcones Fault Zone Aquifer (the Edwards Aquifer) in south-central Texas (Fig. 1) is a karstic aquifer in which groundwater flows through

numerous dissolution channels with high permeability. The Edwards Aquifer has distinct freshwater and saline water zones, and the downdip limit of the freshwater zone is known locally as the "bad-water line" (Fig. 1a). This bad-water line is actually a narrow strip of the transition zone (ranging from < 1 to about 10 km) that occurs along the southern and eastern edges of the freshwater zone where water has been in contact with limestone for a long time. The hydraulic conductivity transitions from an unconfined, hydrologically active freshwater system (90–900 cm/d) to confined, basinal brackish water flow (1–2 cm/d) (Sharp Jr., 1990). The downdip limit of freshwater in the aquifer is the approximate surface defined by the 1000 mg/L total dissolved solids (TDS) concentration. The freshwater (TDS ~ 250–300 mg/L) part of the Edwards Aquifer is approximately 370-km long from west to northeast and about 16 to 65-km wide, bounded to the north by the edge of the recharge zone and to the south and southeast by the downdip limit of freshwater. At the downdip limit of freshwater near San Antonio (TX, USA), the top of the Edwards Aquifer is about 300 m below the land surface, and the aquifer is about 150-m thick (Groschen & Buszka, 1997). The confined aquifer is generally subparallel to the bad-water line, with only diffuse freshwater flowing across the downdip.

Different from the freshwater zone where the host rock is predominately calcitic limestone, the host rock lithology in the saline water zone contains relatively high concentrations of unoxidized organic material, pyrite, gypsum, and celestite (Maclay & Small, 1983; Longman & Mench, 1978) (Fig. 1b). The low permeability of the formation limits the extent of mixing between fresh and saline water, and the long retention time allows the meteoric water interaction with carbonate and evaporite rocks evolving from underlying hydrostratigraphic units and the Edwards Group, reflected by the characteristic Na-Ca-Cl composition saline groundwater in a different area of the saline water zone (Chaudhuri & Ale, 2014). Notably, in the San Antonio metropolitan area, the high Ca, Mg, and SO_4 concentrations in the saline water zone suggest substantial water-rock interaction with carbonate and evaporite dolomitic aquifer rocks (Musgrove et al., 2010). Opsahl and co-workers (Opsahl et al., 2018) also reported the distinctly higher concentration of Cl and Sr in an artesian well near the downdip limit of the freshwater zone, indicating a small extent of mixing with saline groundwater.

While the presence of freshwater and saline water interface in multi-porosity karst aquifers is not uncommon across southern US (Musgrove et al., 2014; Budd and Vacher, 2004; U.S. EPA, 2002), they have mostly

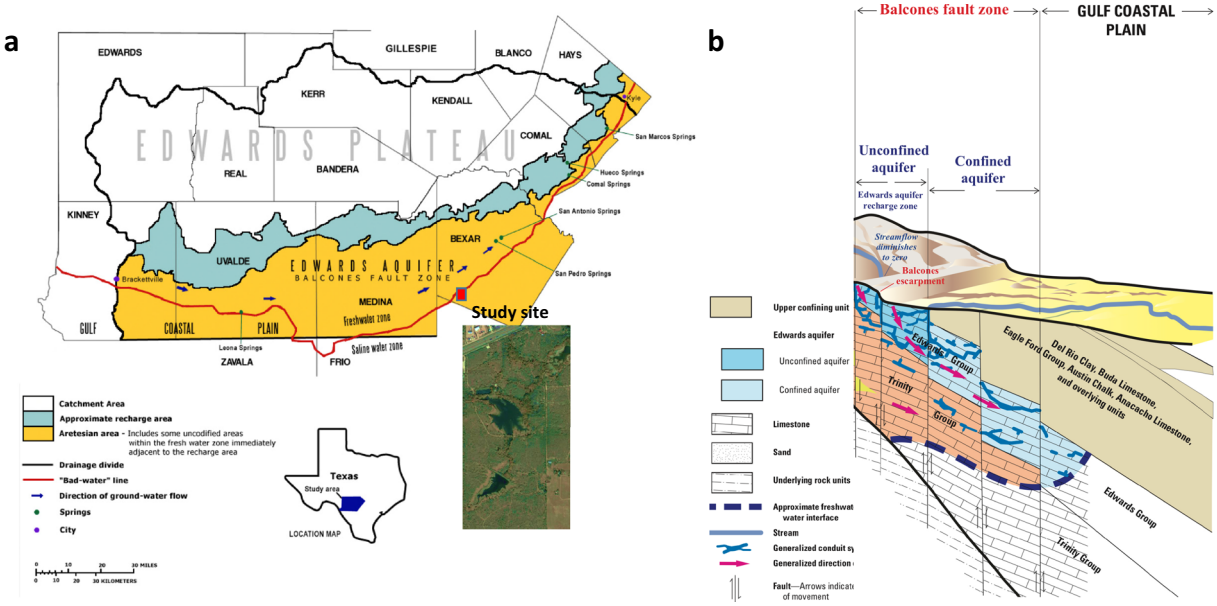

Fig. 1 Hydrogeologic setting in the San Antonio segment of the Edwards aquifer system. (**a**) The approximate boundaries of drainage (catchment) zone, recharge zone, and artesian zone. The red line indicates the "bad-water" line where the "down-dip" fault line splits the aquifer into unconfined and confined sections. The small box (in red) indicates the approximate location of our study site. (**b**) Cross-section view of hydrogeologic framework (not to scale) and generalized groundwater flow directions of the confined and unconfined aquifers in San Antonio region's Balcones fault zone, leading in the southeast direction to Gulf Coastal Plain

been studied from the perspective of regional hydrogeologic characteristics. By comparison, the evolution of deep saline aquifer in a surficial environment has not been investigated, and there exists a knowledge gap concerning how freshwater interference would impact the carbonate and sulfate species emanating from a deep saline aquifer. We hypothesize that freshwater-saline fluid mixing may create a zonation effect with respect to the concentration levels of carbonates and sulfates in the system. However, the kinetic, chemical, and equilibrium fractionation of carbon and sulfur evolution remains to be verified. Therefore, this study aims to profile the evolution of major ions and stable isotopes ($\delta^{13}C_{DIC}$ and $\delta^{34}S_{SO4}$) as water quality indicators at a ranch situated on the immediate saline water side of the bad-water line, near the southwest corner of Bexar County, Texas. The carbon isotope of dissolved inorganic carbon ($\delta^{13}C_{DIC}$) in carbonate species is a reliable indicator to study the geochemical flux in karstic aquifers (Jackson & Polk, 2020; Abongwa & Atekwana, 2015; Abongwa et al., 2016). Additionally, the presence of dissolved H_2S in saline water has been attributed to microbial sulfate reduction associated with petroleum fields along the eastern edge of the aquifer (Oetting et al., 1996), rendering $\delta^{34}S_{SO4}$ to be an effective indicator to study sulfate evolution.

2 Study Area

The study site lies within a 103-ha private ranch (29°15′ 35.13″ N, 98°42′35.13″ W) situated about 28 km southwest of downtown San Antonio, outskirt of the metropolitan area with predominantly revegetated or undeveloped land (Fig. 1a). It is within the narrow transition zone (bad-water line) at the downdip of Edwards Aquifer's freshwater zone. The edge of the Carrizo-Wilcox aquifer runs across the area at a much greater depth underneath the Edwards Aquifer. Additionally, the unregulated oil field brine disposal activities in the early phases of oil production in the Eagle Ford shale play south of the study area has been reported to be the main source of Cl^- and SO_4^{2-} in the Carrizo-Wilcox aquifer. The saline water (TDS > 1000 mg/L) has high concentrations of hydrogen sulfide (H_2S) as a result of geologic brine leakage and possibly also from the nearby oil fields. The 30-year average (1981–2010) annual precipitation for San Antonio is 810 mm. However, rainfall is highly variable in the region, as prolonged dry periods can be punctuated by intense rainfalls. The ranch represents a compelling study location as it situates along the lower edge of the artesian zone of the Edwards Aquifer intersecting with the lower Carrizo-Wilcox Aquifer, while Medina River (the major upstream segment of the San Antonio River) and its tertiary streams channel through the area.

3 Materials and Methods

We collected water samples from 15 locations sequentially totaling a distance of ~ 700 m from the well-head to a distal point in the lake (Fig. 2). At the well-head (site #1), we collected samples by opening the tap. For the rest of the sampling distance, samples were collected by the grab method, and at each sampling point, we made in situ physical and chemical measurements. Prior to collecting the water samples, measurements of temperature, pH, electrical conductivity, and total dissolved solids (TDS) were made using a Yellow Springs Instrument (YSI) multi-parameter probe calibrated to manufacturer's specifications. Water samples collected were filtered through 0.45-μm nylon syringe filters. Samples for anions and cation analyses were collected in high-density polyethylene (HDPE) bottles; the samples for metal analyses were acidified to a pH < 2.0 using high purity HNO_3.

Major anions (Cl^- and SO_4^{2-}) were analyzed using a Dionex Aquion ion chromatograph system at the Water Sciences Laboratory, Texas, A&M University-San Antonio. Major cations (Ca^{2+}, Mg^{2+}, K^+, and Na^+) and trace metals (Sr and Ba) analyses were conducted following USEPA Method 200.7 (U.S. Environmental Protection Agency, 1994), using an Agilent 725 inductively coupled plasma-optical emission spectroscopy (ICP-OES) at the Soil, Water and Forage Analytical laboratory at Oklahoma State University. The analyses of stable isotopes of dissolved inorganic carbon (DIC) ($\delta^{13}C_{DIC}$); H from water (δD_{H2O}); O from water ($\delta^{18}O_{H2O}$); and S from precipitated barium sulfate from water ($\delta^{34}S_{SO4}$) were conducted at the University of Calgary Geosciences, Isotope Science Laboratory (Calgary, Canada). The stable isotope ratios are reported in the standard delta (δ) notation in per mil (‰):

$$\delta(‰) = \left(\left(\frac{R_{sample}}{R_{standard}} \right) - 1 \right) \quad (1)$$

Fig. 2 Sampling locations of the study site. The dots indicate the sampling locations and the line represents the sampling path along which the water quality data are plotted. Land surface samples were collected from well-heads, whereas lake samples were collected by grab sampling just below the water surface

For all isotopic samples, the precision and accuracy at 1-sigma for $n = 10$ was 0.2

The computer program PHREEQC Version 2.8 (Parkhurst & Appelo, 1999) was used to calculate the pCO_2 using pH, temperature, and alkalinity. We also used the computer program PHREEQC to calculate the saturation state with respect to calcite ($SI_{calcite}$) using pH, temperature, alkalinity, and Ca^{2+} concentrations and the saturation state with respect to gypsum (SI_{gypsum}) using pH, temperature, and SO_4^{2-} concentrations.

4 Results

The physical, chemical, and stable isotope results are listed in Table 1.

4.1 pH, Alkalinity, and Total Dissolved Solids (TDS)

The pH, alkalinity, and TDS show a drop in concentrations from the well-head (discharge point at 0 m) to the first approximately 80 m (Fig. 3a–c). After 80 m, the pH values show an increase from 7.82 to 7.94 from 80 to 350 m and stay constant beyond that to the end of the sampling distance (Fig. 3a). The concentrations of alkalinity increased slightly from 123.40 to 128.90 mg/L from 80 to 350 m and stayed constant after that to the end of the sampling distance (Fig. 3b). The TDS concentrations increased slightly from 774.84 to 780.00 mg/L from 80 to 350 m and stayed constant after that to the end of the sampling distance (Fig. 3c). The behavior of the physical parameters shows a three-tier evolutionary stage of sharp decreases in concentrations from 0 to ~ 80 m (Zone 1); slight increases in concentrations from 80 to 350 m (Zone 2); and constant concentration values from 350 m to the end of the sampling distance, 700 m (Zone 3), as shown in Fig. 3.

4.2 Ca, Mg, Na, and K

The Ca concentrations measured an average value of 197 mg/L for the first ~ 80 m with no overall increases or decreases over the 80 m. Beyond 80 m, the Ca concentrations showed a sharp overall drop from 197.30 to 98.80 mg/L from 80 to 270 m, after which, it showed a slight increase to 100 mg/L from 270 to 350 m and dropped slightly to 95.30 mg/L at the end of the sampling distance (Fig. 4a). The Mg concentration showed a minimal increase from 53.40 to 54.20 mg/L for the first ~ 80 m, after which it showed a sharp decreased to 37.10 mg/L from 80 to 210 m. After 210 m, the Mg concentrations decreased slightly from 37.10 to 35.90 mg/L from 210 m to the end of the sampling distance (Fig. 4b). The Na concentration showed an increase from 114.30 to 120.40 mg/L for the first ~ 80 m, after which it showed a sharp decreased to 83.80 mg/L from 80 to 210 m. After 210 m, the Mg concentrations showed a slight increase to 84.40 mg/L to 350 m, after which it decreased from 84.40 to 81.00 mg/L from 350 m to the end of the sampling distance (Fig. 4c). The K concentrations stayed constant at ~ 6 mg/L for the first ~ 80 m, after which it increased sharply from 6 to 12 mg/L from 80 to 210 m and stayed constant at 12 mg/L to the end of the sampling

Table 1 The table shows a description of the sites and the points from which the samples were collected as well as the physical, chemical, isotopic and calculated saturated indices parameters of the sampling locations

Site	Site description	Latitude	Longitude	Distance from WH m	pH	Temp. °C	Alkalinity mg/L as $HCO3^-$	TDS mg/L	Na mg/L	K mg/L
1	Hot tub well-head	29°15′11.71”N	98°42′33.21”W	0	7.98	37	229	1231.54	114.3	6
2	Well-head (WH)	29°15′9.21”N	98°42′37.91”W	15	7.95	36.2	247.7	1267.12	120.5	6
3	10 m from WH	29°15′8.76”N	98°42′37.53”W	20	7.91	34.2	230.2	1247.49	118.2	6
4	20 m from WH	29°15′7.71”N	98°42′37.08”W	30	7.96	33.2	230.8	1256.65	119.4	6
5	30 m from WH	29°15′8.41”N	98°42′37.41”W	50	7.89	31.2	220.1	1246.5	118.5	6
6	40 m from WH	29°15′7.05”N	98°42′36.69”W	60	7.94	30.2	218.5	1240.66	115.9	6
7	50 m from WH	29°15′7.37”N	98°42′37.06”W	70	7.86	28.3	214.9	1252.44	120.7	6
8	60 m from WH	29°15′6.89”N	98°42′36.71”W	80	7.88	27.8	214.1	1249.37	120.4	6
9	Mouth of lake	29°15′6.67”N	98°42′35.71”W	110	7.89	21.8	159.6	994.99	99.9	9
10	Pond A	29°15′5.47”N	98°42′35.37”W	210	7.82	16.9	123.4	774.84	83.8	12
11	Pond B	29°15′2.86”N	98°42′36.64”W	270	7.89	17.7	122.2	771.54	84.3	12
12	Pond C	29°15′0.24”N	98°42′39.74”W	350	7.94	16.4	128.9	780.12	84.4	12
13	Pond D	29°15′1.11”N	98°42′36.12”W	480	7.93	14.7	124.1	784.74	82.3	12
14	Pond E	29°15′2.65”N	98°42′32.28”W	700	7.93	14.6	123.3	784.08	81	12

Site	Ca mg/L	Mg mg/L	Cl mg/L	SO_4^{2-} mg/L	B mg/L	Sr mg/L	$\delta^{13}C_{DIC}$‰	$\delta^{18}O_{H2O}$ ‰	$\delta^{34}S_{H2O}$ ‰	log $p_{CO2(g)}$ atm.	$SI_{calcite}$	SI_{gypsum}
1	197.9	53.4	215	415.9	0.44	7.25	1.51	‰	20.01	−2.53	1.21	−0.8
2	195.1	54.1	216.1	427.7	0.45	7.39	1.79	−4.33	20.8	−2.46	1.2	−0.8
3	198.2	53.6	215.1	426.2	0.45	7.29	−1.5	−4.32	20.75	−2.47	1.11	−0.79
4	201.7	54	214.5	430.2	0.45	7.39	0.85	−4.24	20.06	−2.52	1.16	−0.78
5	201.8	53.6	211.6	434.9	0.45	7.42	0.53	−4.12	20.58	−2.48	1.05	−0.77
6	199	54.5	213.9	432.7	0.44	7.49	0.45	−4.15	20.18	−2.54	1.07	−0.78
7	200.5	54.5	210.2	445.5	0.46	7.41	0.34	−4.05	20.07	−2.48	0.97	−0.76
8	197.3	54.2	215.7	441.6	0.45	7.44	−0.1	−3.99	20.06	−2.5	0.97	−0.77
9	149.5	45.7	191.1	340	0.36	5.66	2.22	−3.97	20.07	−2.67	0.7	−0.92
10	98.8	37.1	163.4	238	0.28	4.15	6.27	0.03	23.51	−2.72	0.32	−1.16
11	98.8	36.9	163.3	239.6	0.28	4.14	6.65	3.49	23.18	−2.79	0.39	−1.16
12	100	37.1	163.9	237.9	0.28	4.05	6.53	3.68	23.6	−2.83	0.45	−1.16
13	95.7	36.3	163.1	229.8	0.27	4.04	6.44	3.68	23.62	−2.84	0.39	−1.18
14	95.3	35.9	162	228.8	0.27	3.98	6.43	3.42	23.65	−2.85	0.38	−1.18

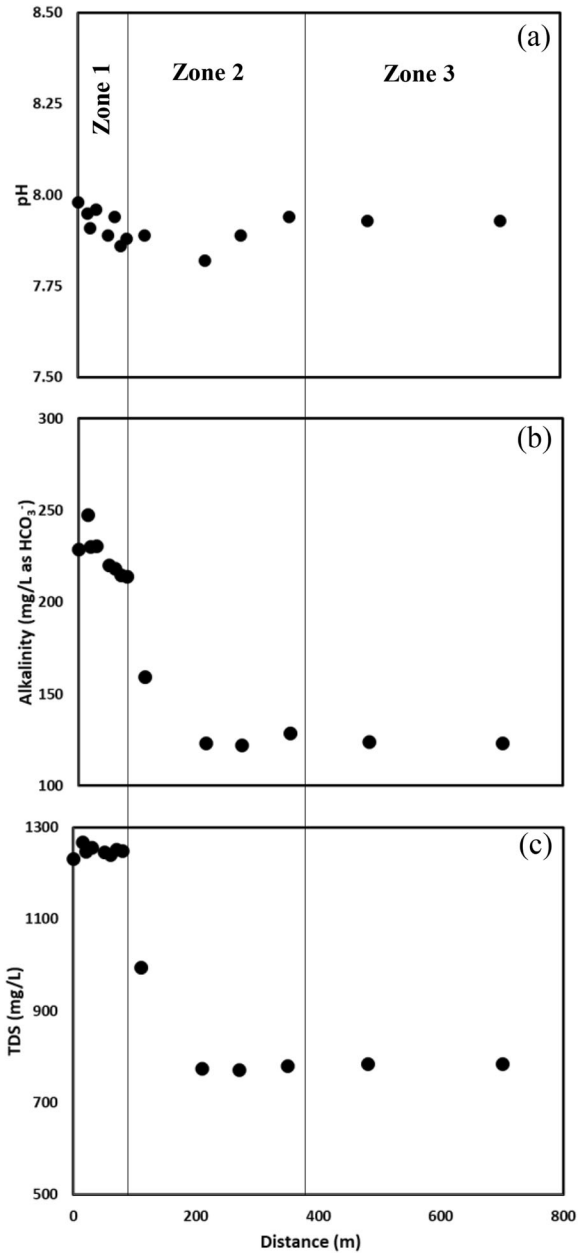

Fig. 3 The pH (a), alkalinity (b), and total dissolved solids (TDS) (c) concentrations of the samples over distance. The concentrations show a three-tier evolutionary pattern over distance: Zone 1 (0–80 m) is dominated by the deep fluid; Zone 2 (80–210 m) is the mixing zone of fresh-ponded water and deep fluid; and Zone 3 (210–700 m) is the fresh-ponded water

distance (Fig. 4d). The major ions showed a three-tier evolutionary stage over distance in almost identical distances as mentioned under physical parameters in Section 4.2. We have grouped these evolutionary stages into three zones: 0–80 m (Zone 1); 80 to 210 m (Zone 2); and 210 m to the end of the sampling distance at 700 m (Zone 3), as shown in Fig. 4.

4.3 Sr and B

The Sr concentrations showed an increase from 7.25 to 7.44 mg/L for the first ~ 80 m, after which it showed a sharp decrease from 7.44 to 4.15 mg/L from 80 to 210 m. After 210 m, the Sr concentrations showed a slight continuous decrease from 4.15 to 3.98 mg/L from 210 m to the end of the sampling distance, 700 m (Fig. 5a). The B concentrations showed a very minimal increase from 0.44 to 0.45 mg/L from 0 to 80 m, after which its concentration decreased sharply from 0.45 to 0.28 mg/L from 80 to 210 m. Beyond 210 m, the concentration of B decreased ever so slightly from 0.28 to 0.27 mg/L from 210 m to the end of the sampling distance (Fig. 5b). The evolution of the trace metals (Sr and B) shows a three-tier pattern divided into various zones based on distances, Zone 1 (0–80 m), Zone 2 (80–210 m), and Zone 3 (210–700 m), as shown in Fig. 5.

4.4 SO_4^{2-} and Cl^-

The SO_4^{2-} concentrations showed a continuous increase from 415.90 to 441.60 mg/L from 0 to 80 m and sharp decrease in concentrations from 441.60 to 238.0 mg/L from 80 to 210 m. Beyond 210 m, the SO_4^{2-} concentrations showed a slow continuous decrease from 238 to 228.80 mg/L from 210 m to the end of the sampling distance (Fig. 6a). The Cl^- concentrations did not show any major net increase or decrease for the first ~ 80 m, staying at an average concentration of 215.00 mg/L. From 80 to 210 m, the Cl^- concentrations dropped significantly from 215.7 to 163.40 mg/L and showed a continuous but slight decrease from 163.4 to 162.00 mg/L from 210 m to the end of the sampling distance (Fig. 6b). The anions also mirrored a three-tier evolutionary pattern over distances as shown in Figs. 3, 4, and 5.

4.5 $\delta^{13}C_{DIC}$, $\delta^{34}S_{SO4}$, $\delta^{18}O_{H2O}$, and δD_{H2O}

The $\delta^{13}C_{DIC}$ showed continuous enrichment from − 1.79 to − 0.10‰ for the first 80 m, and showed a sharp and major decrease in the carbon isotopic values from − 0.10 to −6.27‰ from 80 to 210 m. Beyond 210 m, the $\delta^{13}C_{DIC}$ continue to decrease from − 6.27 to − 6.43‰

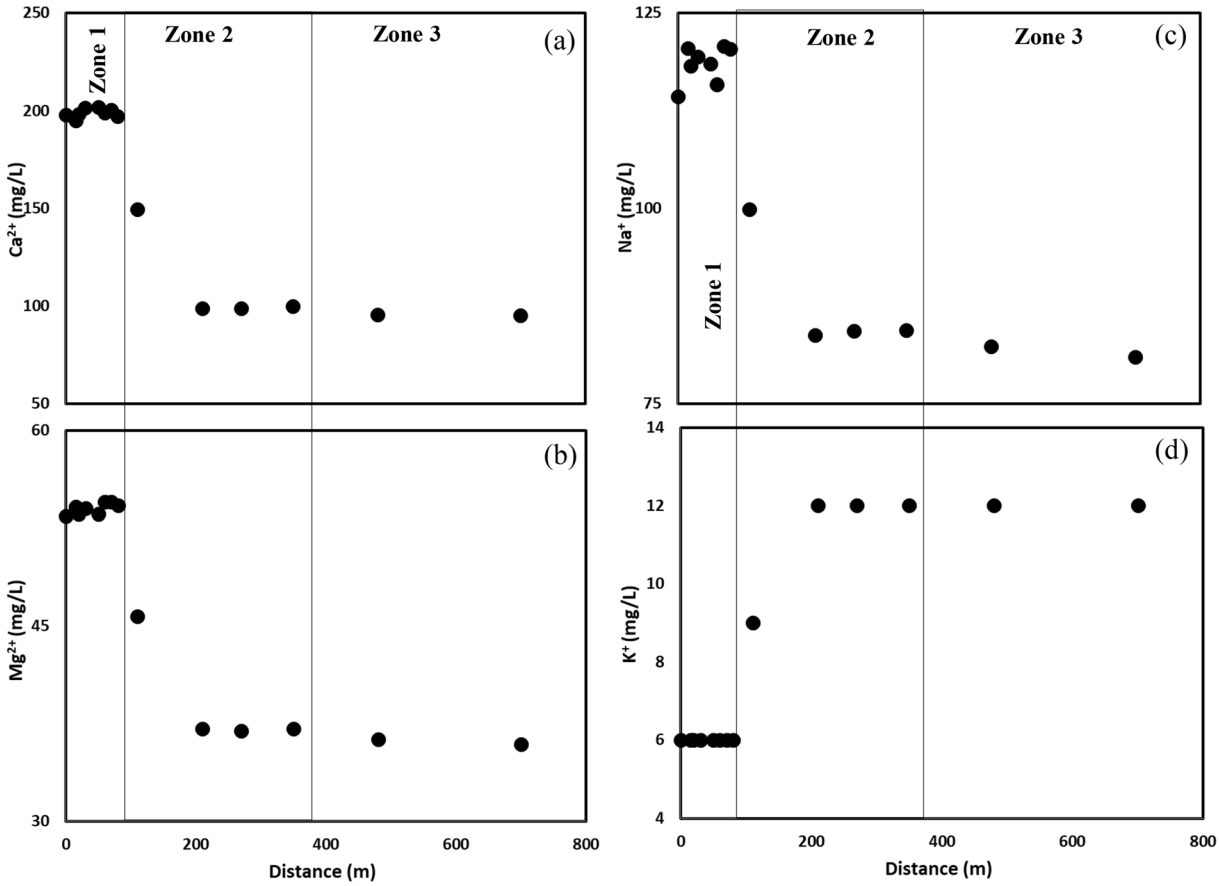

Fig. 4 The Ca^{2+} (a), Mg^{2+} (b), Na^{+} (c), and K^{+} (d) concentrations of the samples over distance, showing the three-tier evolutionary behaviors

from 210 m to the end of the sampling distance (Fig. 7a). The $\delta^{34}S_{SO4}$ showed a + 1.16 ‰ enrichment for the first ~ 20 m from + 19.59 to +20.75‰, after which, the $\delta^{34}S_{SO4}$ values dropped from + 20.75 to + 20.07‰ from 20 to 80 m. From 80 to 210 m, the $\delta^{34}S_{SO4}$ showed marked enrichment from + 20.07 to + 23.50‰, beyond which point, the $\delta^{34}S_{SO4}$ showed a slight but continued enrichment from +23.50 to +23.65 ‰ from 210 m to the end of the sampling distance (Fig. 7b). The $\delta^{18}O_{H2O}$ showed continuous enrichment from − 4.33 to − 3.97‰ for the first 80 m and showed a sharp and major enrichment of + 7.46‰ from 80 to 210 m with the $\delta^{18}O$ values increasing from − 3.97 to +3.49‰. Beyond 210 m, the $\delta^{18}O$ continue to be enriched though slightly, from + 3.49 to +3.57‰ from 210 m to the end of the sampling distance (Fig. 7c). The δD_{H2O} showed a continuous but minimal enrichment of 1.22‰ from 0 to 80 m with the values increasing from − 25.57 to − 24.35‰, after which, the δD showed a major enrichment of + 13.25‰ from 80 to 210 m increasing from − 24.57 to + 11.10‰. Beyond 210 m, the δD continued to be enriched though slightly, from + 11.10 to + 10.52‰ from 210 m to the end of the sampling distance (Fig. 7d). The evolutionary behaviors of the stable isotopes reflect the three-tier pattern exhibited by the physical and chemical parameters.

5 Discussion

5.1 Hydro-Biogeochemical Characteristics

5.1.1 $\delta^{18}O_{H2O}$ and δD_{H2O} Characterization of the Three-Tier Evolutionary Trend

The distinct zones and the three-tier evolution observed are a result of the geo-chemical composition of the deep fluid as it gets modified during its evolution. Zone 1 is characterized mainly by deep groundwater that has evolved from rainfall which recharges the aquifer. The

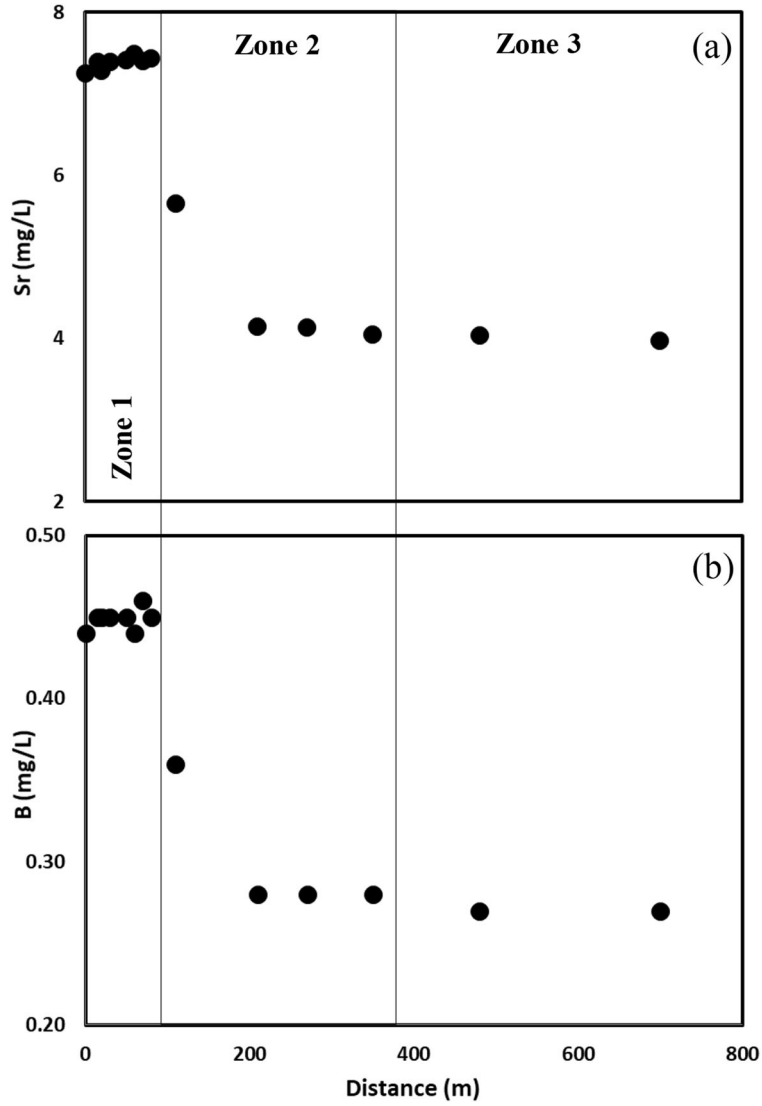

Fig. 5 The Sr (a) and B (b) concentrations of the samples over distance, showing the three-tier evolutionary behaviors

measured δD and $\delta^{18}O$ of the deep fluid at the well-head to the first 80 m (Zone 1) can be compared to the local meteoric water line (LMWL) relationship defined by the line $\delta D = 0.859\delta^{18}O - 21.47$ (Fig. 8). The calculation was derived from San Antonio rain samples collected in January of 2020, and these values show a characteristic depleted value for recharge with apparently no evaporation effect. As observed, in Zone 1 the $\delta^{18}O$ values ranged from −4.33 to −3.97‰ and the δD values ranged from −25.57 to −24.35‰ which are sitting on the LMWL. Any variation from the LMWL as we progressively trace its spatial evolution would therefore illustrate a modification of the isotopes due to processes such as mixing, evaporation, or isotopic exchange. Zone 2 (80 to 210 m) indicates an area of mixing where the isotopic signatures begin to modify into lighter isotopes, with the $\delta^{18}O$ values ranging from −3.97 to +0.03 ‰ and the δD values ranging from −24.35 to −5.00‰, indicating some influence from water with a more isotopically light isotope (e.g., Hedley et al., 2009). As we move further away from the well-head into the ponded-open water surface, the effects of evaporation become more pronounced and progressively enrich the remaining water in heavy isotopes ($\delta^{18}O$ values ranging from +3.49 to +3.57‰ and the δD values ranging from +10.52 to +11.10‰), resulting in the deep fluid/surficial and ponded-water evaporative water line (SPEWL) shift away from the LMWL to produce a lower regression

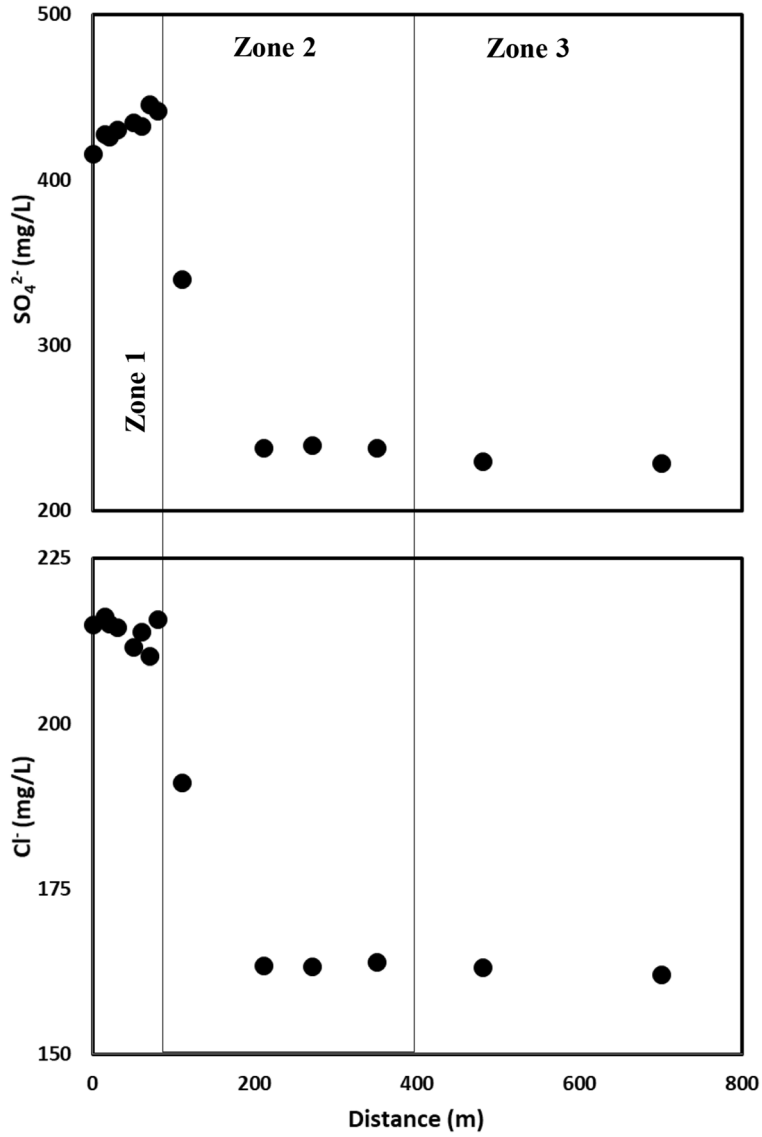

Fig. 6 The SO_4^{2-} (a) and Cl^- (b) concentrations of the samples over distance, showing the three-tier evolutionary behaviors

slope, $\delta D = 4.668\,^{18}O - 5.396$ (Fig. 8). The results (Table 2) by Musgrove et al. (2019) showed that the confined and transient zone (Fig. 1) of the Edwards Aquifer all has similar chemical and isotopic parameters, but these parameters get modified as they flow over land and are influenced by other water sources and by evaporation. Central Texas climate is subhumid to semi-arid (Larkin & Bomar, 1983), and this would have marked effect on the modification of the significantly lighter isotopes that recharges the aquifer immediately they are discharge into surface environments. The ponded water (Zone 3) is exposed to the atmosphere and therefore affected by the evaporation resulting in the enrichment of the water with heavier isotopes as the lighter isotopes escape from the system.

5.1.2 Carbonate Evolution

Decreasing pH and alkalinity were observed for the first 80 m from the well-head (Fig. 3a and b), and the decreasing concentrations of HCO_3^- were also associated with decreasing $pCO_{2(g)}$ (Table 1). The dissolution of the aquifer materials resulted in $pCO_{2(g)}$ concentrations ($10^{-2.53}$ atm) being higher than atmospheric ($10^{-3.50}$ atm), causing CO_2 loss through pressure differential and leading to decreasing pH and alkalinity. Chemical

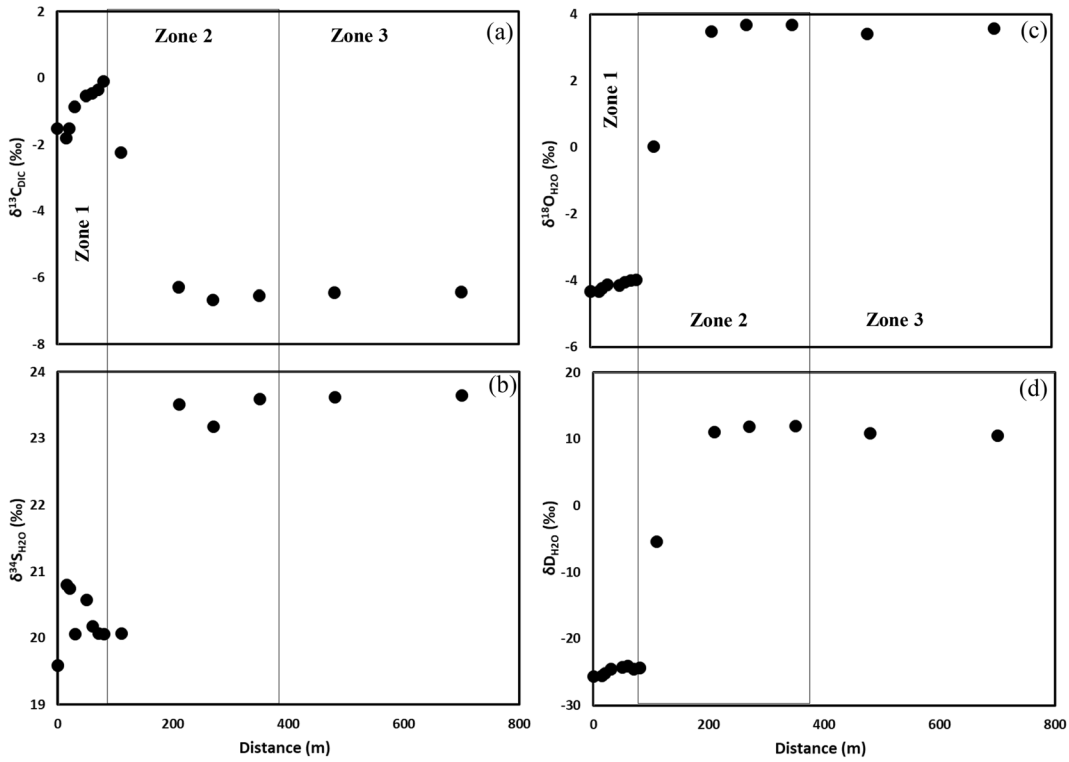

Fig. 7 The carbon isotopic ratio of dissolved inorganic carbon ($\delta^{13}C_{DIC}$) (a); the sulfate isotopic signatures ($\delta^{34}S_{SO4}$) (b); the oxygen isotopes of the water samples ($\delta^{18}O_{H2O}$); and the hydrogen isotopic signatures of the water samples (δD_{H2O}) (d), over distance showing the three-tier evolutionary behaviors over distance distinguished in Zones 1–3

reactions (2) to (5) depict the dissolution of CO_2 in the form of H_2CO_3 that loses protons through acid equilibria, resulting in the observed reduction of pH over distance.

$$CaCO_{3(s)} + CO_{2(aq)} + H_2O \longrightarrow Ca^{2+}{}_{(aq)} + 2HCO_3^-{}_{(aq)}$$

$$CO_{2(aq)} + H_2O \longrightarrow H_2CO_{3(aq)}$$

$$H_2CO_{3(aq)} \longrightarrow H^+{}_{(aq)} + HCO_3^-{}_{(aq)}$$

$$HCO_3^-{}_{(aq)} \longrightarrow H^+{}_{(aq)} + CO_3^{2-}{}_{(aq)}$$

To understand the behavior of carbon from deep fluid carbon-rich water in surficial environments, we need to determine when carbon is removed from the system. Several authors (e.g., Dandurand et al., 1982; Pentecost, 1995) have demonstrated that carbon removal from carbonate-rich waters is controlled by either $CO_{2(g)}$ outgassing or carbon scavenging from solution via carbon-mineral precipitation. To elucidate the controlling factors of carbon evolution in the system, we plotted the normalized alkalinity (i.e., alkalinity at any time, $alkalinity_t$, divided by the alkalinity at the discharge point, $alkalinity_0$) as a function of the $pCO_{2(g)}$ for the entire sampling distance (Fig. 9). Doctor et al. (2008) have demonstrated that decreasing alkalinity and decreasing

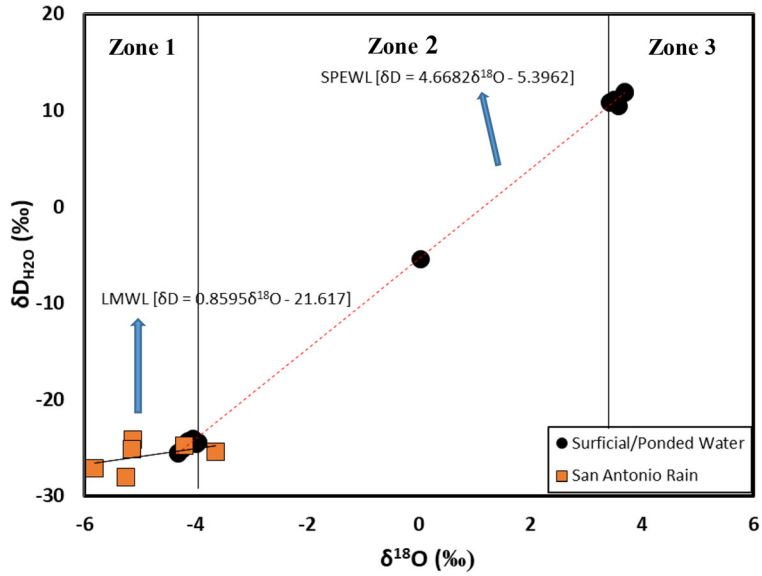

Fig. 8 Plots showing the local meteoric water line (LMWL) constructed from San Antonio, TX, rain samples collected by this author between Dec. 2019 and Jan. 2020 and the deep fluid/surficial and ponded-water evaporation line (SPEWL) constructed from the O and H isotopes of the surficial fluid and ponded-water. The result show that the surficial water is derived from the groundwater and that the ponded water has been significantly modified by evaporation

$pCO_{2(g)}$ are caused by outgassing of excess dissolved CO_2 due to the high initial $CO_{2(g)}$ concentration in the solution. We observed a rapid decrease in the alkalinity and $pCO_{2(g)}$ for the first 80 m (Zone 1), followed by a slow decrease beyond the 80-m mark (Zone 2) (Fig. 9). This result indicates that the amount of dissolved $CO_{2(aq)}$ in a carbon-dominated system is the main control of the evolution of carbon in such systems. As shown in Fig. 8, the zone labeled (1) indicates the stretch with high dissolved $pCO_{2(g)}$, and that labeled with (2) represents the transition zone (zone of mixing). Beyond this point, the zone labeled (3) indicates the zone with relatively low $pCO_{2(g)}$, and the trajectory showed that the reduction in alkalinity values is less steep than in the zone labeled (1). Beyond the 80-m mark (Zone 2), the system had lost most of its dissolved $CO_{2(g)}$ due to $CO_{2(g)}$ pressure differentials, resulting in a flattened alkalinity curve in (Zone 3) as observed in Fig. 3b.

Carbonate system parameters can constrain the conditions required for carbonate precipitation, as decreasing $pCO_{2(g)}$ is associated with increasing carbonate mineral solubility in pure water systems (e.g., Drever, 1997; Langmuir, 1997; Morse & Mackenzie, 1990). Fluid mixing and $CO_{2(g)}$ loss from surficial carbonate-rich waters are the main drivers of increased calcite saturation states. As the deep groundwater emerges with relatively higher $pCO_{2(g)}$ concentrations ($10^{-2.53}$ atm) than the atmospheric ($10^{-3.50}$ atm), the exsolution of $CO_{2(g)}$ causes the waters to reach approximately 30 times saturation in calcite. Calculated saturation indices of calcite ($SI_{calcite}$) showed that the system was supersaturated with respect to calcite, suggesting that the continuous calcite saturation sequestered carbon into the system through calcite mineral precipitation. This process leads to decreasing alkalinity values over distance (Fig. 10a). For the first ~ 80 m (Zone 1) of the sampling distance, the degassing of CO_2 was controlled mainly by waters derived from carbonate dissolution. Beyond this point (Zone 2), fluid mixing played a major role, as there was a sharp increase in the $pCO_{2(g)}$ concentrations and a sharp decrease in alkalinity. The system would suddenly approach a state of equilibrium (Zone 3) with respect to calcite. The decreasing $pCO_{2(g)}$ with decreasing $SI_{calcite}$ values (Fig. 10b) beyond Zone 1 indicates that the loss of carbon is controlled by the mixing of the ponded water with the emanated groundwater. The ponded water exhibits low relatively $pCO_{2(g)}$ concentrations and low relatively TDS that is likely also sourced from rain and the groundwater. Furthermore, carbonate growth kinetics is inhibited by Mg^{2+} concentrations (e.g., Suarez, 1983; Zhang & Dawe, 2000). With a Mg^{2+}/Ca^{2+} ratio of ~ 0.27 for the first ~ 210 m (Zone 1) and ~ 0.38 beyond the 80-m mark (Zone 2), the results show that the concentrations of Mg^{2+} played a major role in the precipitation of calcite in Zone 1 but a minimal role in calcite precipitation in Zone 3 as indicated in Fig. 10c.

5.1.3 Sulfate Evolution

The Edwards Aquifer' saline zone has a mineral composition more diverse than that of its freshwater zone.

Table 2 Selected geochemical and isotopic constituents from five wells in the confined section of the Edwards Aquifer (Musgrove et al., 2019)

Site	Site description	Latitude	Longitude	pH	Temp. °C	Alkalinity mg/L	TDS mg/L	Na mg/L	K mg/L	Ca mg/L	Mg mg/L	Cl mg/L	SO4 mg/L	B µg/L	Sr µg/L	$\delta^{13}C_{DIC}$ ‰	$\delta^{18}O_{H2O}$ ‰	δD_{H2O} ‰	$SI_{calcite}$	SI_{gypsum}
PSW1	Confined aquifer/well	29.54178	,-98.63556	7	22.5	334.0	360	10.80	1.20	105.0	14.0	17.9	24.7	50.0	414	−8.97	−4.2	−23.30	−0.06	−2.06
PSW2	Confined aquifer/well	29.49528	,-98.59556	7.2	27	242.0	300	13.30	1.30	71.0	18.8	26.5	33.6	61.5	1730	−7.70	−4.2	−24.80	−0.01	−2.06
Z-DED	Confined aquifer/well	29.49528	,-98.59556	6.9	22	322.0	350	11.10	1.50	95.0	17.7	17.5	28.2	58.0	517	−9.15	−4.1	−22.70	−0.08	−0.10
Comal 1	Confined/spring orifice	29.71278	,-98.13750	7.1	23.5	288.0	344	14.00	1.40	87.0	17.0	20.4	39.7	72.5	628	−9.21	−4.2	−23.30	−2.04	−1.92

*PSW public supply well

The samples were collected from 2013 to 2017 and the results presented are the median ($n = 30$)

Although calcite and dolomite are the dominant mineral compositions of the Edwards Aquifer's confined zone, minerals such as gypsum, anhydrite, celestite, and strontianite are present in lesser amounts in this zone (e.g., Opsahl et al., 2018). Circulating water within the rocks of the confining beds dissolve gypsum and anhydrite, producing relatively higher concentrations of sulfate. The concentration of sulfate measured (~416 mg/L) at the discharge point (0 m) of the study site, which is in Edwards Aquifer's confined zone, was about ten times higher than the averaged maximum measured sulfate concentration in the unconfined up-dip zone (e.g., Opsahl et al., 2018). The sulfate concentrations and the calculated gypsum saturation index (SI_{gypsum}) from Musgrove et al. (2019), measured from the four wells (PSW1, PSW2, Z-DED, and Comal 1; Table 2), are of similar values to the measured and calculated values presented in this research, indicating that the sources of the water in the confined section of the Edwards Aquifer are similar, but the water gets sufficiently modified during its evolution in surficial environments. In the surficial environment, the dissolved sulfate concentrations increased continuously for the first ~80 m; beyond this point, the SO_4^{2-} concentration dropped abruptly at the 110-m mark before flattening out in the mixing zone and evaporated influenced ponded water (Fig. 11a). Sulfate mineral precipitation can scavenge dissolved sulfate from solutions, sequestering them in sulfate minerals such as gypsum and anhydrite. However, calculated saturation indices of gypsum (SI_{gypsum}) showed that the system was under-saturated with respect to gypsum, thereby suggesting that the increasing concentrations of sulfate in the first ~80 m from the discharge point was controlled by the dissolution of gypsum or anhydrite beds in the aquifer. To show the relationship between sulfate concentrations and sulfate mineral precipitation, we plotted the SI_{gypsum} vs. SO_4^{2-} concentrations (Fig. 11b). The plot shows that the under-saturation with respect to gypsum is associated with both increasing and decreasing sulfate concentrations. Figure 11c, a plot of the concentration of sulfate at any time ($SO_4^{2-}{}_t$) divided by the concentration of sulfate at the discharge point ($SO_4^{2-}{}_0$) as a function of distance (i.e., $SO_4^{2-}{}_t/SO_4^{2-}{}_0$ vs. distance), shows that the increasing sulfate concentration in the first ~80 m (Zone 1) is due to the high sulfate concentrations emanating from the discharge point, and that the decreasing concentration beyond Zone 1 into the mixing area (Zone 2) and the freshwater (evaporated) pond (Zone 3) is as result of

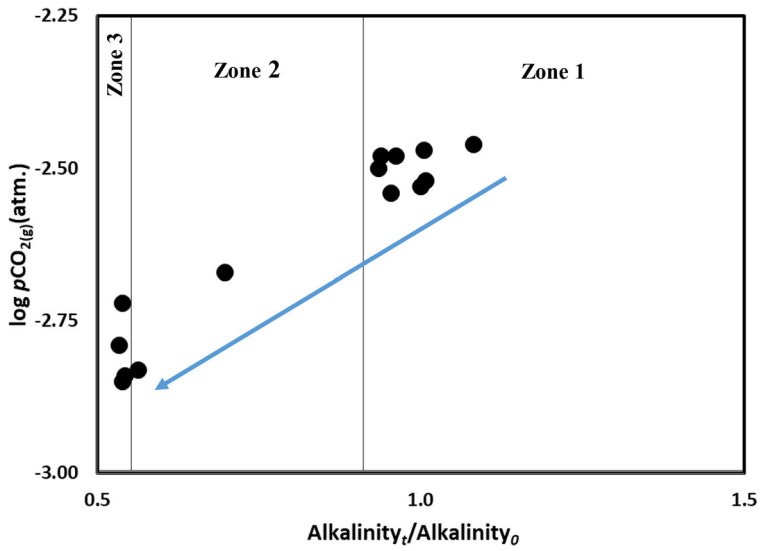

Fig. 9 Plot of $pCO_{2(g)}$ vs the alkalinity concentration at any time (alkalinity$_t$) divided by the alkalinity at the well-head (alkalinity$_0$), i.e., $pCO_{2(g)}$ vs. alkalinity$_t$/alkalinity$_0$. The plot shows an overall decreasing alkalinity concentration across the three zones because of the continuous $CO_{2(g)}$ evasion due to the higher than atmospheric $pCO_{2(g)}$ of the system

fluid mixing with water of lower TDS that has been diluted by rain.

Sulfate-reducing bacteria are known to be O_2-tolerant – especially in the absence of H_2S – and could form toxic products with O_2 when they remain viable for hours or even days (e.g., Hardy & Hamilton, 1981; Fukui & Takii, 1990). These deep fluids are often associated with the presence of bacterial mats on stream beds and well-heads. Several authors (e.g., Cohen, 1989; Canfield & DesMarais, 1991) have reported that the observed microbial mats in oxic environments were responsible for sulfate reduction. Therefore, we hypothesize that the presence of both aerobic and anaerobic bacteria in the oxic environment over the entire sampling distance has utilized H_2, organic compounds, and sulfur compounds as electron donors for microaerophilic respiration. This process would oxidize sulfides to sulfates and result in the high sulfate concentrations measured at the well-head and the first ~ 80 m of the sampling distance (Zone 1).

5.2 Isotopic Evolution

5.2.1 $\delta^{13}C_{DIC}$ Evolution

To understand the carbon isotopic ($\delta^{13}C_{DIC}$) behavior, we plot the ratio of alkalinity$_t$/alkalinity$_0$ as a function of $\delta^{13}C_{DIC}$ (Fig. 12). We intended to demonstrate how changing alkalinity and isotopic fractionation in a continuously evolving water sample would change in an alkalnity-$\delta^{13}C$ space (Abongwa & Atekwana, 2013). We observe a rapid decrease in the alkalinity accompanied by kinetic isotopic fractionation resulting in a $\delta^{13}C_{DIC}$ enrichment of ~ 1.75‰ in Zone 1 (Fig. 12). The accompanied kinetic isotopic fractionation is due to the loss of excess $CO_{2(g)}$ as a result of the higher $pCO_{2(g)}$ concentrations in the deep fluid compared to that in the atmospheric (e.g., Mills & Urey, 1940; Usdowski & Hoefs, 1990). Evasion of $CO_{2(g)}$ results in decreasing calcite super-saturation to cause a $\delta^{13}C_{DIC}$ decrease from 0.10 to − 6.43‰ as observed after the 80-m mark, as represented in Zones 2 and 3 (Fig. 12). Our results show that, although carbonate evolution for the deep fluid indicates a supersaturated system, the main driving force for the carbon isotopic fractionation is controlled by kinetic equilibrium fractionation generated by higher concentrations of dissolved carbonate species. In a continuum, the fractionation of carbonate species in a supersaturated carbonate system is controlled mainly by kinetic isotopic fractionation observed in the zones labeled as 1 in the figures. Moreover, as the system becomes diluted with isotopically heavier water ($\delta^{18}O$ and δD) as a result of evaporation, and with relatively lower dissolved carbonate species concentrations, the shifts in fractionation become more negative (Zone 2; Fig. 12) and then show no fractionation as the curve flattens out in Zone 3 (Fig. 8). In stages 2 and 3 of Fig. 12, the change in carbonate species concentrations (decreasing alkalinity

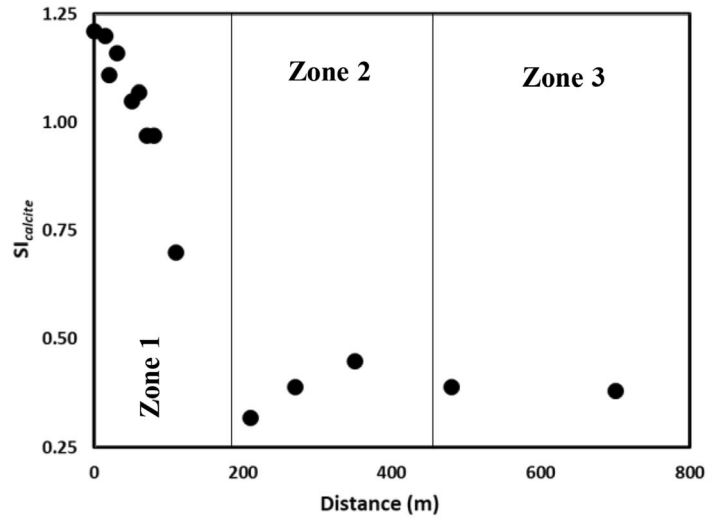

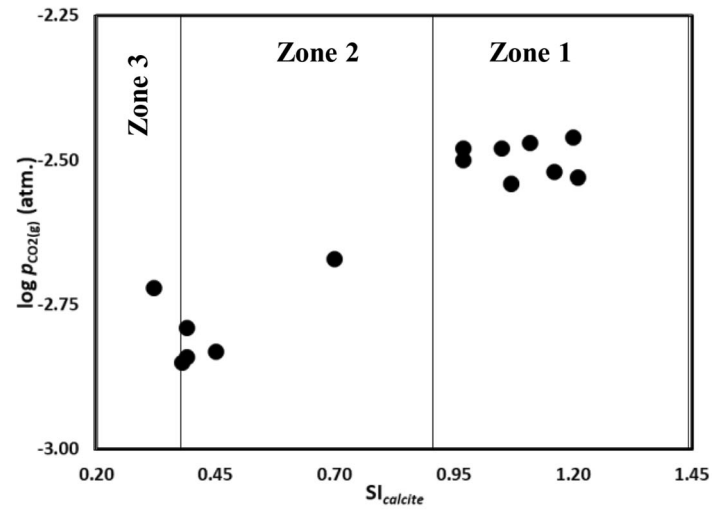

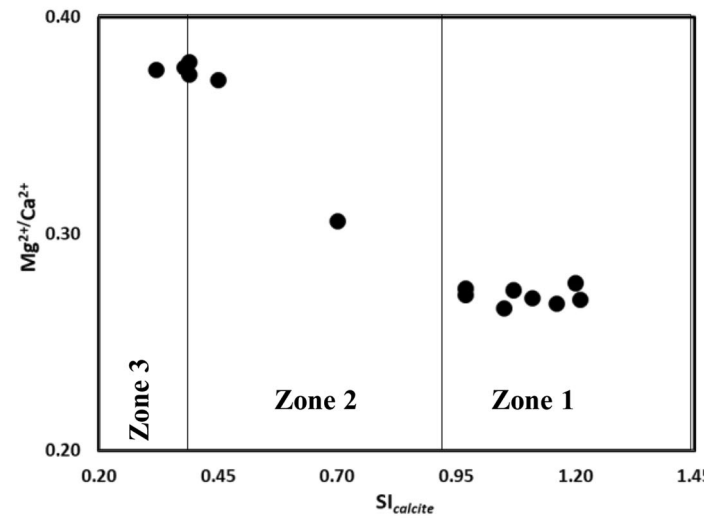

Fig. 10 (a) Plot of calculated saturated indices of calcite ($SI_{calcite}$) showing that the system is supersaturated with respect to calcite across the three zones. (b) Plot of $pCO_{2(g)}$ vs $SI_{calcite}$ showing calcite mineral precipitation as $CO_{2(g)}$ outgasses. (c) Plot of Mg^{2+}/Ca^{2+} vs. $SI_{calcite}$ showing that carbonate calcite mineral precipitation scavenges Ca^{2+} from the system

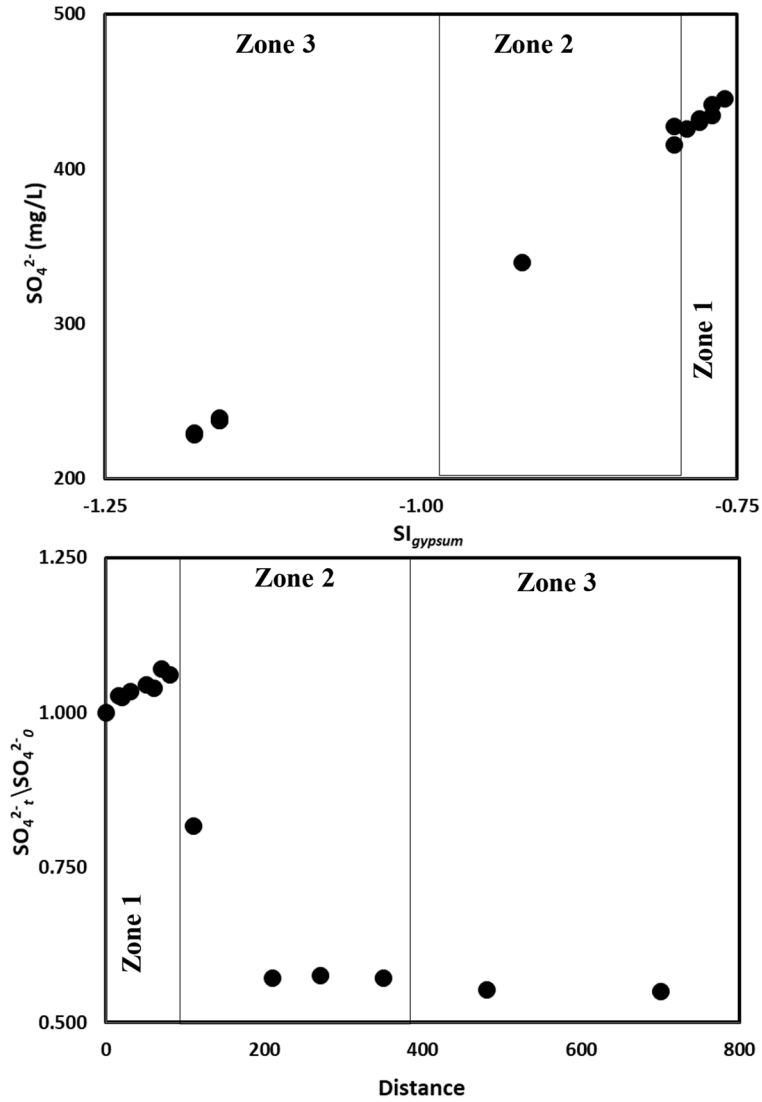

Fig. 11 A Plot of the concentrations of SO_4^{2-} vs. calculated gypsum saturated indices (SI_{gypsum}) showing that the system might not be precipitating gypsum, and a plot of SO_4^{2-} concentrations at any time ($SO_4^{2-}{}_t$) divided by SO_4^{2-} concentration at the well-head ($SO_4^{2-}{}_0$), i.e., $SO_4^{2-}{}_t/SO_4^{2-}{}_0$, over distance, indicating that the sharp drop in SO_4^{2-} concentrations at Zones 2 and 3 are due to mixing by relatively low sulfate-rich ponded freshwater (b)

observed in Zone 2) is not accompanied by kinetic fractionation. We hypothesize that there is very minimal loss of $CO_{2(g)}$ after 80 m because the system is diluted with less carbonate- rich water; no observable enrichment in kinetic isotopic fractionation is made. Additionally, because the system is still far from achieving equilibrium fractionation, carbon isotopic enrichments cannot shift positively. Several authors (e.g., Usdowski et al., 1979; Dandurand et al., 1982) have suggested that equilibrium precipitation of calcite should result in a $\delta^{13}C_{DIC}$ enrichment shift of about 0.9‰. Such results were not observed in this study because the system was highly diluted by carbonate-depleted water.

5.2.2 $\delta^{34}S_{SO4}$ Evolution

The $\delta^{34}S_{SO4}$ values of the groundwater at the well-head were ~ 20.01‰, indicating that the sulfate in the groundwater is sourced from evaporites. The results of $\delta^{34}S_{SO4}$ are very different from meteoric water, which varies between − 1.4 and + 6.9‰, but similar to the seawater sulfur isotopic composition of 20.9‰ (e.g., Rees et al., 1978; Rech et al., 2003). To understand sulfur isotopic fractionation and track its evolution, we plotted the concentration ratio of time-dependent SO_4^{2-} to its concentration at the well-head, as a function of $\delta^{34}S_{SO4}$ (i.e., $SO_4^{2-}{}_t/\ SO_4^{2-}{}_0$ vs. $\delta^{34}S_{SO4}$) in Fig. 13. The $\delta^{34}S_{SO4}$ values showed a slight overall enrichment (~ 0.3‰) in

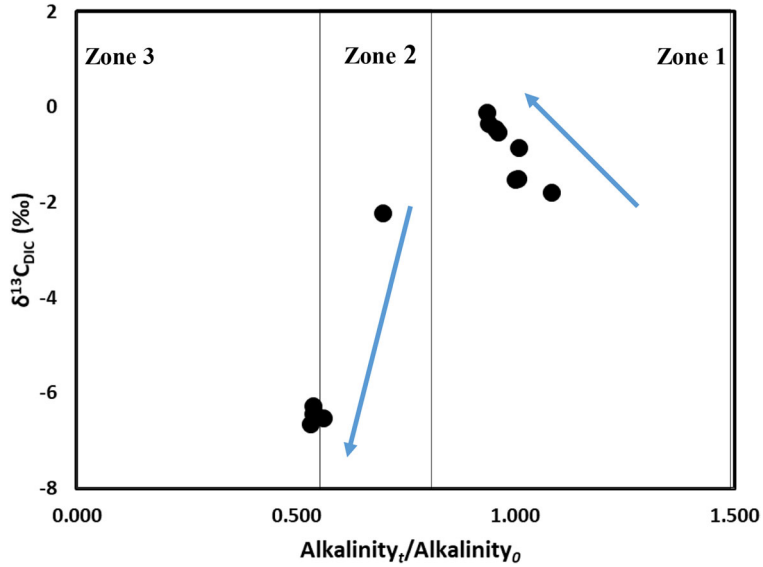

Fig. 12 Plot of carbon isotopic signatures of dissolved inorganic carbon ($\delta^{13}C_{DIC}$) vs. alkalinity$_t$/alkalinity$_0$, showing that CO2 outgassing reduces alkalinity concentration while causing a positive shift in $\delta^{13}C_{DIC}$ values in Zone 1. Mixing of fresh-ponded water with deep fluid in Zones 2 and 3 results in a negative shift in $\delta^{13}C_{DIC}$ values

the first ~ 80 m (Zone 1), whereas the SO_4^{2-} concentration increased from 451 to 442 mg/L. This increase in sulfate concentration with minimal overall isotopic enrichment could be attributed to the fact that the system was not scavenging sulfate from the solution through sulfate metal precipitation, as shown in Fig. 11a, since the $SI_{calcite} < 0$. Beyond the first 80 m, we observed a sharp enrichment of $\delta^{34}S_{SO4}$ from 20.07 to 23.51‰, and the system continued to show enrichment to a value of 23.65‰ at the end of sampling distance. This sharp increase in $\delta^{34}S_{SO4}$ matches the point where the fresh-ponded water starts to mix with the sulfate-rich deep fluid, resulting in a reduction in sulfate concentration to the end of the sampling distance as seen in Zones 2 and 3 of Fig. 13. The continuous enrichment of $\delta^{34}S_{SO4}$ beyond 80 m results in a + 2.4‰ shift, which could be accounted for by the microbial reduction of thiosulfate to sulfides. The overall enrichment of $\delta^{34}S_{SO4}$ over distance supports the hypothesis that microbial metabolism is responsible for the sulfates reduction to sulfides. The broad environmental distribution of sulfate-reducing bacteria (Postgate, 1979) implies that anaerobes could operate in the fresh-water pond and the mixing zone since some of these microbes have high oxygen tolerance.

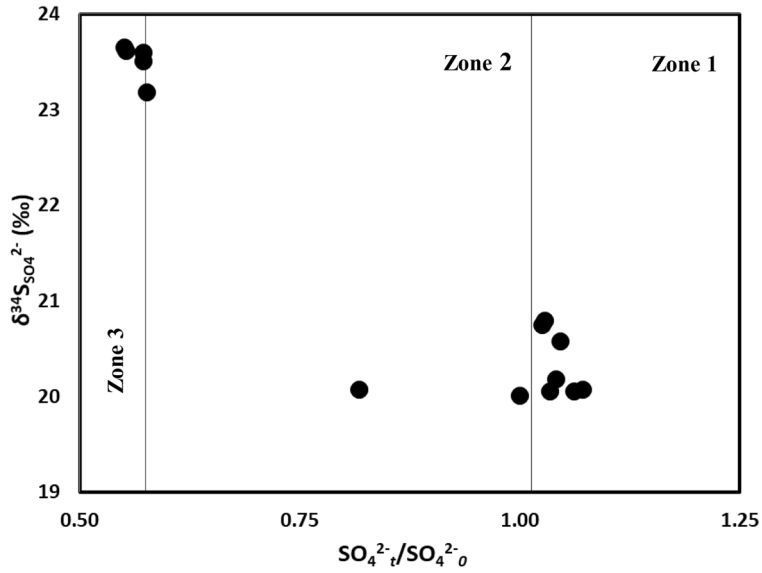

Fig. 13 Plot of sulfate isotopic signature of the water ($\delta^{34}S_{SO4}$) vs. $SO_4^{2-}{}_t/SO_4^{2-}{}_0$ indicating that the concentrations of SO_4^{2-} is in Zone 1 are controlled by microbial metabolism resulting to isotopic fractionation and that sulfate fractionation is almost absent in Zones 2 and 3 because of the influence of fresh-ponded water

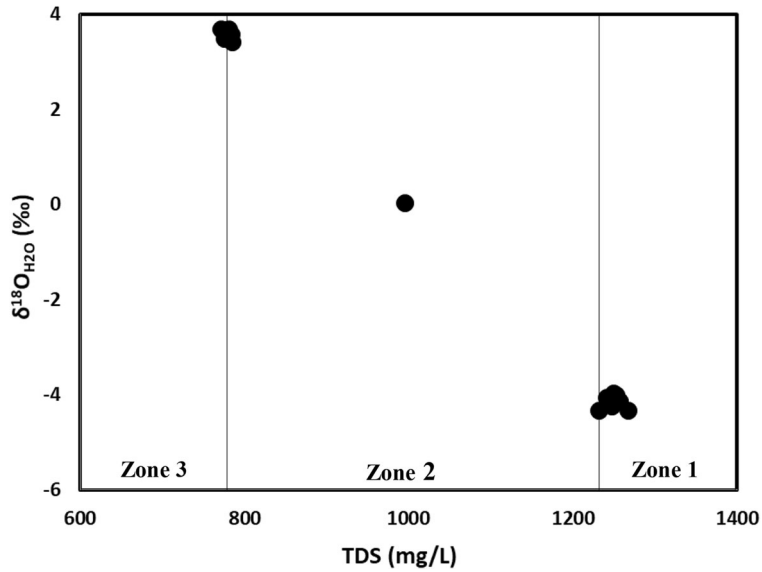

Fig. 14 Plot of oxygen isotope of the water ($\delta^{18}O_{H2O}$) vs. the total dissolved solids (TDS). The figure shows that evapo-concentration plays a role in the increasing TDS concentration observed in Zone 1, and the decreasing TDS and enrichment of $\delta^{18}O_{H2O}$ in Zones 2 and 3 are as a result of the mixture of low-solute fresh-ponded water with the deep fluid

5.2.3 Evaporative Fractionation

The effects of evaporative concentration on the geochemical evolution of deep fluid in surficial environments are shown in a plot of TDS versus $\delta^{18}O_{H2O}$ (Fig. 14). The results show an increase in TDS with a corresponding enrichment in $\delta^{18}O_{H2O}$ for the first ~ 80 m (Zone 1; Fig. 14). Beyond this distance, the TDS concentration decreases with a corresponding enrichment in $\delta^{18}O_{H2O}$. This result could be explained by the fact this is the area (Zones 2 and 3) where relatively limited solutes-rich fresh-ponded water mixes with the sulfate-rich deep fluid. The increase in TDS for the first ~ 80 m (Zone 1) of the sampling distance exhibits a positive log-normal relationship typical to evaporated river water (e.g., Atekwana et al., 2016). Thus, the decreasing TDS concentrations with continuous enrichment in $\delta^{18}O_{H2O}$ (Zones 2 and 3; Fig. 14) are indicative of the phenomenon that there is deep fluid dilution by freshwater and no solute addition through water-rock interactions. The decreasing $\delta^{13}C_{DIC}$ in Zones 2 and 3 (Fig. 12) suggests that the corresponding fractionation of the isotopes are not controlled by evapo-concentration (e.g., Farquhar et al., 1989; Walker & Richardson, 1991).

6 Conclusions

The study site locating at the immediate saline water zone allows the researchers to study how deep fluid emanating from the Edwards Aquifer's confined saline zone evolves in a surficial environment. We demonstrated that the evolution of carbonates and sulfates in such fluids in a surficial environment could be tracked by the accompanying isotopic fractionation resulting from $CO_{2(g)}$ evasion, sulfate mineral precipitation, microbial respiration, and evapo-concentration, all within a small stream-pond water system. Of significance in the evolutionary process is the role of microbes where, through metabolism, they convert sulfates to thiosulfates resulting in the microbial fractionation of sulfate-rich fluids. We therefore suggest that the evolution of sulfates- and carbonates-rich fluids in these surficial environments is controlled primarily by kinetic-isotopic fractionation and microbial metabolism. The role of evaporation in the fractionation process of the $\delta^{18}O$ and δD is very pronounced in the enrichment shifts observed as the deep fluid evolved from the well-head to the mixing zone and, finally to the freshwater evaporative water zone. As the studied stream-pond system is typical of the water supply sources for ranches and well-owners along the saline-confined zone of the aquifer, our study also bears important public health implications concerning the need for longer retention in surficial environment and freshwater dilution.

Acknowledgements We thank Samantha Gonzales and Karla Tapia for assisting in the sample collection and analyses. We also thank Dr. Shray Saxena for running the anions sample.

Funding This research was supported financially by the Texas A&M University-San Antonio, Research Council Grants 2018/2019 and 2019/2020, and the Texas A&M University-San Antonio, College of Arts and Science Summer Grants 2019 and 2020.

References

Abongwa, P. T., & Atekwana, E. A. (2013). Assessing the temporal evolution of dissolved inorganic carbon in waters exposed to atmospheric $CO_{2(g)}$: A laboratory approach. *Journal of Hydrology, 505*, 250–265.

Abongwa, P. T., & Atekwana, E. A. (2015). Controls on the chemical and isotopic composition of carbonate springs during evolution to saturation with respect to calcite. *Chemical Geology, 404*, 136–149.

Abongwa, P. T., Atekwana, E. A., & Puckette, J. (2016). Dissolved inorganic carbon and stable carbon isotopic evolution of neutral mine drainage interacting with atmospheric $CO_{2(g)}$. *Science of the Total Environment, 545*, 57–66.

Atekwana, E. A., Molwalefhe, L., Kgaodi, O., & Cruse, A. M. (2016). Effect of evapotranspiration on 569 dissolved inorganic carbon and stable carbon isotopic evolution in rivers in semi-arid climates: The 570 Okavango Delta in North West Botswana. *Journal of Hydrology: Regional Studies, 7*, 1–13.

Budd, D. A., & Vacher, H. L. (2004). Matrix permeability of the confined Floridan aquifer, Florida, USA. *Hydrogeology Journal, 12*, 531–549.

Canfield, D. E., & DesMarais, D. J. (1991). Aerobic sulfate reduction in microbial mats. *Science, 251*, 1471–1473.

Chaudhuri, S., & Ale, S. (2014). Temporal evolution of depth-stratified groundwater salinity in municipal wells in the major aquifers in Texas, USA. *Science of the Total Environment, 472*, 370–380.

Cohen, Y. (1989). Photosynthesis in cyanobacterial mats and its relation to the sulfur cycle: A model for microbial sulfur interactions. In Y. Cohen & E. Rosenberg (Eds.), *Microbial mats: Physiological ecology of benthic microbial communities* (pp. 22–36). American Society of Microbiology.

Dandurand, J. L., Gout, R., Hoefs, J., Menschel, G., Schott, J., & Usdowski, E. (1982). Kinetically-controlled variations of major components and carbon isotopes in a calcite-precipitating spring. *Chemical Geology, 36*, 299–315.

Doctor, H. D., Kendall, C., Sebestyen, S. D., Shanley, T. B., Ohte, N., & Boyer, E. N. (2008). Carbon isotope fractionation of dissolved inorganic carbon (DIC) due to outgassing of carbon dioxide from a headwater stream. *Hydrological Processes, 22*, 2410–2423.

Drever, J. I. (1997). *The geochemistry of natural waters: Surface and groundwater environments*. Prentice Hall 436 pp.

Farquhar, G. D., Ehleringer, J. R., & Hubick, K. T. (1989). Carbon isotope discrimination and 614 photosynthesis. *Annual Review of Plant Biology, 40*, 503–537.

Fukui, M., & Takii, S. (1990). Survival of sulfate-reducing bacteria in oxic surface sediment of a seawater lake. *FEMS Microbiology Ecology, 73*, 317–322.

Groschen, G. E., & Buszka, P. M. (1997). Hydrogeologic framework and geochemistry of the Edwards Aquifer saline-water zone, South-Central Texas. U.S. Geological Survey: Water-Resources Investigations Report 97–4133.

Hardy, J. A., & Hamilton, W. A. (1981). The oxygen tolerance of sulphate reducing bacteria isolated from North Sea waters. *Current Microbiology, 6*, 259–262.

Hedley, P., Dogramaci, S., & Dodson, W. (2009). The use of major ion analysis and stable isotopes O^{18} and H^2 to distinguish groundwater flow in Karijini National Park, Western Australia.

Jackson, L., & Polk, J. S. (2020). Seasonal delta C-13(DIC) sourcing and geochemical flux in telogenetic epikarst of south-Central Kentucky. *Earth Surface Processes and Landforms, 45*, 785–799.

Langmuir, D. (1997). *Aqueous environmental geochemistry*. Prentice-Hall 600 pp.

Larkin, T. J., & Bomar, G. W. (1983). *Climatic atlas of Texas. Texas Department of Water Resources* (p. 151). Limited Printing Report LP–192.

Longman, M., & Mench, P. A. (1978). Diagenesis of cretaceous limestones in the Edwards aquifer system of south-Central Texas: A scanning electron microscope study. *Sedimentary Geology, 21*, 241–276.

Maclay, R. W., & Small, T. A. (1983). Hydrostratigraphic subdivisions and fault barriers of the Edwards aquifer, south-Central Texas, USA. *Journal of Hydrology, 61*, 127–146.

Mills, A., & Urey, H. C. (1940). The kinetics of isotope exchange between carbon dioxide, bicarbonate ion, carbonate ion, and water. *Journal of American Chemical Society, 62*, 1019–1026.

Morse, J. W., & Mackenzie, F. T. (1990). *Geochemistry of sedimentary carbonate*. Elsevier.

Musgrove, M., Stern, L. A., & Banner, J. L. (2010). Springwater geochemistry at Honey Creek State natural area, central Texas: Implications for surface water and groundwater interaction in a karst aquifer. *Journal of Hydrology, 388*, 144–156.

Musgrove, M., Katz, B. G., Fahlquist, L. S., Crandall, C. A., & Lindgren, R. J. (2014). Factors affecting public-supply well vulnerability in two karst aquifers. *Groundwater, 52*, 63–75.

Musgrove, M., Solder, J. E., Opsahl, S. P., & Wilson, J. T. (2019). Timescales of water-quality change in a karst aquifer, south-Central Texas. *Journal of Hydrology X, 4*, 100041.

Oetting, G. C., Banner, J. L., & Sharp Jr., J. M. (1996). Regional controls on the geochemical evolution of saline groundwater in the Edwards aquifer, Central Texas. *Journal of Hydrology, 181*, 251–283.

Opsahl, S. P., Musgrove, M., Mahler, B., & Lambert, R. B. (2018). Water-quality observations of the San Antonio segment of the Edwards aquifer, Texas, with an emphasis on processes influencing nutrient and pesticide geochemistry and factors affecting aquifer vulnerability, 2010-16 (no. 2018–5060). US Geological Survey.

Parkhurst, D. L., & Appelo, C. A. J. (1999). User's guide to PHREEQC (Version 2.1)-a computer program for speciation, batch-reactions, one-dimensional transport and inverse geochemical calculations. U.S. Geological Survey, Water Resource Investigation Report, 99–4256.

Pentecost, A. (1995). Geochemistry of carbon dioxide in six travertine-depositing waters in Italy. *Journal of Hydrology, 167*, 263–278.

Postgate, J. R. (1979). *The sulphate-reducing bacteria* (p. 17). Cambridge University Press.

Rech, J. A., Quade, J., & Hart, W. S. (2003). Isotopic evidence for the source of Ca and S in soil gypsum, anhydrite and calcite in the Atacama Desert, Chile. *Geochimica et Cosmochimica Acta, 67*, 575–586.

Rees, C. E., Jenkins, W. J., & Monster, J. (1978). The sulphur isotopic composition of ocean watersulphate. *Geochimica et Cosmochimica Acta, 42*, 377–381.

Sharp Jr., J. M. (1990). Stratigraphic, geomorphic and structural controls of the Edwards Aquifer, TX, USA. In E. S. Simpson & J. M. Sharp Jr. (Eds.), *International Association of Hydrogeologists, selected papers for the 28th International Geological Congress, Vol. 1* (pp. 67–82). Heise Hannover.

Suarez, D. L. (1983). Calcite supersaturation and precipitation kinetics in the lower Colorado River, all American canal and east highline canal. *Water Resource Research, 19*, 653–661.

U.S. Environmental Protection Agency. (1994). Method 200.7: Determination of metals and trace elements in water and wastes by inductively coupled plasma-atomic emission spectrometry. Revision 4.4. Cincinnati, OH, U.S.A..

United States Environmental Protection Agency. (2002). Delineation of source-water protection areas in karst aquifers of the ridge and valley and Appalachian plateaus physiographic provinces: Rules of thumb for estimating the capture zones of springs and wells. EPA 816-r-02-015. Washington D.C., U.S.A..

Usdowski, E., & Hoefs, J. (1990). Kinetic $^{13}C/^{12}C$ and $^{18}O/^{16}O$ effects upon dissolution and outgassing of CO_2 in the system CO_2-H_2O. *Chemical Geology, 80*, 109–118.

Usdowski, E., Hoefs, J., & Menschel, G. (1979). Relationship between ^{13}C and ^{18}O fractionation and changes in major element composition in recent calcite-depositing spring- A model of chemical variations with inorganic $CaCO_3$ precipitation. *Earth and Planetary Science Letters, 42*, 267–276.

Walker, C. D., & Richardson, S. B. (1991). The use of stable isotopes of water in characterizing the source 717 of water in vegetation. *Chemical Geology, 94*, 145–158.

Zhang, Y., & Dawe, R. A. (2000). Influence of Mg^{2+} on the kinetics of calcite precipitation and calcite crystal morphology. *Chemical Geology, 163*, 129–138.